The Net Zero Mass Loss Phenomenon on Opening Switching Contacts with AC Loading

Jonathan Swingler and John W. McBride

***Abstract*—Studies are conducted on silver metal oxide contacts on a purposed built apparatus to investigate the extent of contact erosion under opening (break) operations. The contacts are opened between 0.1 and 0.8 ms^{-1} at particular point-on-wave, t_{POW}, of the ac waveform. Current loading of up to 30 A rms, I_{rms}, is investigated. Contact material deposition, as well as mass loss, is observed and is found to balance at particular current values and point-on-wave opening leading to a net zero mass loss on the contacts. Results are presented on mass change for each contact against the two parameters of current and point-on-wave. An arc duration characteristic, ζ, is plotted against current, I_{rms}, which has a net zero mass loss. The characteristic is shown to be the same for both silver tin oxide and silver cadmium oxide but is influenced by the opening velocity. The metallic and gaseous ion transfer mechanisms of the arc discharge are presented as the main processes behind this phenomenon.**

***Index Terms*—AC arc erosion, oxide contacts, silver metal.**

NOMENCLATURE

D_g	Mass gain due to gaseous ion transfer mechanism/ng.
ε_m	Mass loss due to metallic ion transfer mechanism/ng.
I_{rms}	Applied current (rms)/A.
K	Erosion/deposition constant of proportionality/ $s^2\mathrm{m}^{-1}\mathrm{A}^{-1}$.
M_a	Mass change on anode per opening operation/ng.
$P(I_{\mathrm{rms}}, t)$	Power/W.
$R_g(t, v^{-1})$	Gaseous transfer function.
$R_m(I_{\mathrm{rms}})$	Metallic transfer function.
t	Time/ms.
t_{POW}	The point-on-wave that the contacts are opened, τ-ζ/ms.
τ	Half duty cycle, 10 ms.
v	Opening velocity/ms^{-1}.
V	Arc voltage/V.
ζ	Arc duration to produce net zero mass change on a contact/ms.

Manuscript received October 22, 1997; revised January 1, 1999. This paper was recommended for publication by Guest Editor M. Braunovic upon evaluation of the reviewers' comments. This paper was presented at the 43rd IEEE Holm Conference on Electrical Contacts, Philadelphia, PA, October 20–22, 1997..

The authors are with the Departments of Mechanical Engineering and Electrical Engineering, Electro-Mechanical Research Group, University of Southampton, Southampton S017 1BJ, U.K.

Publisher Item Identifier S 1521-3331(99)03282-1.

I. INTRODUCTION

THERE are two major concerns with electrical contacts fitted in switches and switchgear:

1) erosion of the contact material on make or break (closing or opening the contact pair);
2) contact welding which prevents switching taking place [1], [2].

The amount of erosion dictates the useful lifetime of the contact pair and occurs due to material transfer by several phenomena, the arc discharge being the most dominant for opening contacts under an electrical load. A particular contact that has undergone arc erosion can have either a net mass loss or gain depending on the polarity of the contact and the nature of the arcing process such as duration [3]–[6].

The amount of erosion on a contact caused by dc arcs has been related to the length and duration of the arc. The "anodic arc" is named because it leads to extensive erosion on the anode. This type of arc is usually short in length and duration, and is associated with resistive loads. In contrast, the "cathodic arc" is usually longer, leading to extensive cathode erosion. This type of arc has been particularly associated with inductive loads and takes place after a period of anodic arc behavior [7], [8]. If the contact pair is in close proximity, material can be transferred from one contact to the other with no apparent loss to the environment. This phenomenon of a transfer of material from the anode to the cathode has been called "anodic erosion" and transfer of material from the cathode to the anode has been called "cathodic erosion" [6].

A lengthening arc as it is drawn between opening contacts is known to go through several different arc phases (or stages) resulting in an anodic and cathodic arc behavior. Each phase has its own distinctive mass removal rate and deposition rate for a contact. Additionally, features in the arc voltage/time characteristic [9]–[13] have indicated the transition between phases.

Fig. 1 shows schematically the arc voltage/time characteristic for a contact pair opened with a direct current supply. Initially on opening, the contact force reduces resulting in heating at the interface leading to the creation of a molten bridge [14]. On further opening, the bridge ruptures causing transfer of material from the bridge to the contact surfaces. The bridge may rupture asymmetrically resulting in mass loss on one contact

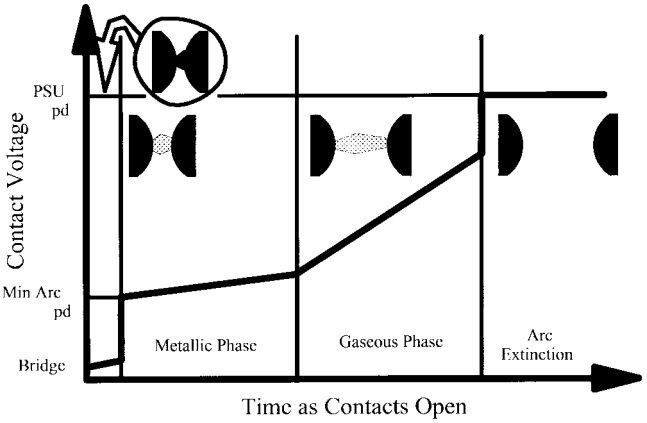

Fig. 1. Arc phases.

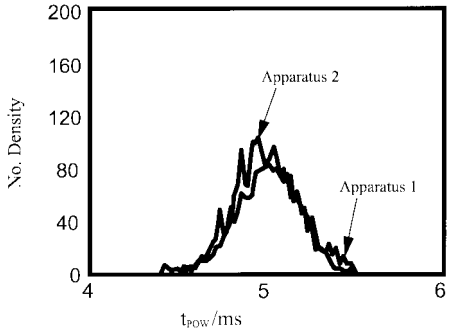

Fig. 2. Distribution of hits at 5 ms point-on-wave.

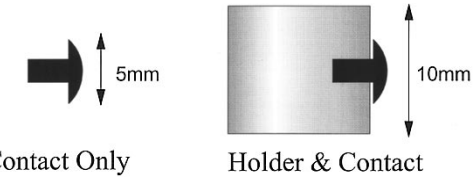

Fig. 3. The contact holder is able to collect arc deposits.

and gain on the other. After the rupture, the remaining contact gap is heavily filled with vaporized contact metal which is ionized leading to the arc discharge. The arc has been reported to go through at least two phases [15], [16], the metallic phase and the gaseous phase, before extinguishing. From a mechanistic perspective, the metallic phase (indicated in Fig. 1) involves the anode being eroded by electron bombardment releasing metal vapor into the gap causing a mass loss. This vapor can undergo ionization producing positively charged metallic ions. These metallic ions are accelerated in the electric field toward the cathode and deposited due to the high cohesive ability between species of same type [16]. This causes a mass gain at the cathode. Chen *et al.* have described this in the particle sputter-depositing model (PSD) [15], [16]. Additionally, metallic vapor and recombined metallic ions can deposit on the contacts. As a result of this mechanism, described here as the metallic ion transfer mechanism, there is a net transfer of contact material from the anode to the cathode. As the contacts are opened further, atmospheric gases diffuse into the discharge and are ionized producing positively charge gaseous ions. On further opening, the plasma becomes dominated with these gaseous ions and the arc enters the second phase, the gaseous phase (see Fig. 1). The gaseous ions are accelerated toward the cathode and sputter it releasing vaporized contact material into the gap. The vaporized material mainly deposit onto the anode, resulting in a net transfer from the cathode to the anode. This mechanism is called the gaseous ion transfer mechanism.

The metallic ion transfer mechanism dominates at the beginning of the drawn arc discharge and can lead to transfer of material from the anode to the cathode (anodic erosion). The gaseous ion transfer mechanism dominates later in the drawn arc discharge and can lead to transfer of material from the cathode to the anode (cathodic erosion). Ben Jemaa *et al.* have investigated the transition between the two types of arc behavior and report a critical arc length of between 15–30 μm, a few times the electron free path [17]. By controlling the arc duration on opening an ac supply at particular current loading, the two mechanisms governing these two types of arc behavior can be shown to balance resulting in net zero mass loss. The net zero mass loss does not however correspond to zero erosion of the surface as material is either redeposited or transferred from the opposing contact [18].

II. Experimental Procedure

A. The Break Apparatus

The experimental facility used in this study consists of two break test rigs. One of these has been previously reported [19]. Each test rig is used to conduct horizontal break opening operations on a pair of contact samples. The rate of operation is eight breaks per minute, at an opening velocity, v, of: -0.1, 0.3, 0.5, 0.7, and 0.8 ± 0.01 ms^{-1}. Alternating current of 50 Hz, $I_{\rm rms}$, of: -5.6, 9.3, 14.7, 26.3, and 30.8 A rms is used at 240 V rms under resistive loading. The current was allowed to flow for 370 ± 10 ms before the contacts are opened at a prescribed point on the current waveform, called the point-on-wave, $t_{\rm pow}$, of: -1, 3, 5, and 7 ms. The precision of the point-on-wave opening is illustrated in Fig. 2 for 2000 operations at $t_{\rm pow} = 5$ ms for the two test rigs. The profile is typical for other $t_{\rm pow}$ values. Voltage and current measurements are taken every 10 μs during the opening operations.

Contact samples used in this study were Ag/SnO_2 contact rivet pairs (no dopants) along with Ag/CdO contact rivet pairs previously studied by Abu Sharkh and McBride [20], [21].

B. Sample Analysis Techniques

Mass measurements are taken of contact samples before and after 5000 break operations to determine mass loss or gain of that contact at a particular current and point-on-wave. The mass measurement technique used for the Ag/SnO_2 data presented involved measuring only the contact rivet whereas in the previously published work for Ag/CdO [20] the mass measurement technique included weighing the contact and its holder. This new technique is adopted to improve the accuracy of the mass measurement. By including the holder, material that deposited onto the holder from the arc discharge is included giving a false reading of mass gain on the rivet. Fig. 3 indicates the potential area for collecting material from the arc discharge. The holder and contact arrangement is able to

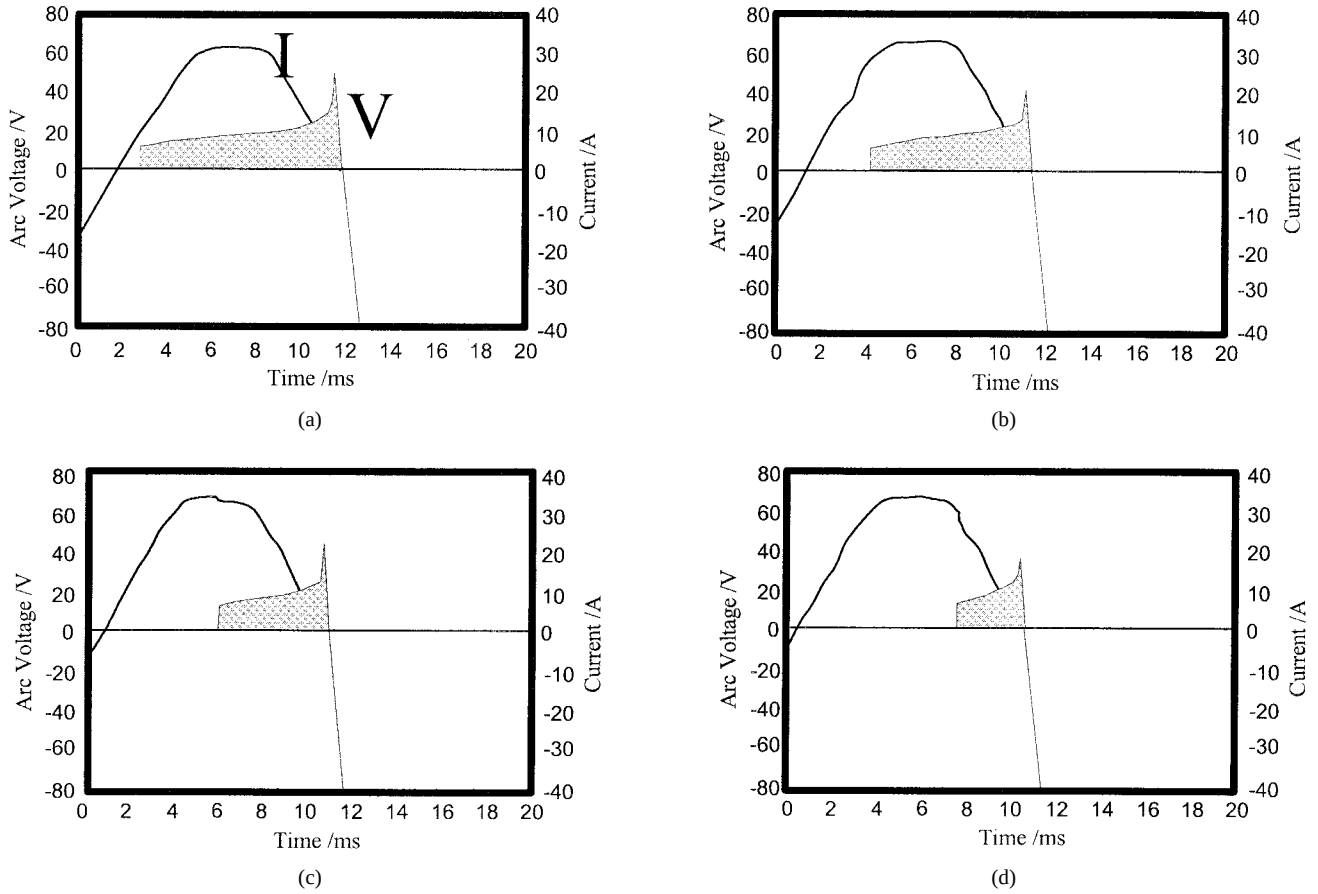

Fig. 4. Current/voltage characteristics of Ag/SnO_2 contacts opening with an arc.

collect >98% of radially expanding material from the contact gap, a minimal amount is lost to the environment, compared to the contact rivet which is able to collect ∼85% [6]. However, the mass measurement of the holders, which contain contact material deposits, proved useful in the study as will be shown in the results.

III. Experimental Results

A. Voltage/Current Characteristics

Voltage/current characteristics are taken of each opening operation. Fig. 4 show these for Ag/SnO_2 samples tested at 26.3 A rms, 0.1 ms^{-1}, and opened at 1, 3, 5, and 7 ms into the current waveform. It can be seen that the current waveform remains sinusoidal with a slight perturbation during the discharge. At different current values studied, the current profile is similar and only differed in magnitude. Arc voltage profiles for different $t_{\rm POW}$ at $I_{\rm rms} = 26.3$ A are shown in Fig. 4. The profiles exemplify features which are seen at different current for respective $t_{\rm POW}$. The voltage magnitude for the respective current and $t_{\rm POW}$ has approximately the same value.

B. Mass Change Data, M_a

1) Ag/SnO_2 Anode and Cathode at 0.1 ms^{-1} Opening Velocity: The anode and cathode of each contact pair are weighed to determine the amount of material gained or lost. Fig. 5 shows the mass change data, M_a, of each sample (a positive value as gain and a negative value as loss) plotted in two types of graph, a 3-D plot and contour plot. The mass change data is plotted against the $I_{\rm rms}t_{\rm POW}$ plane, i.e., the current ($I_{\rm rms}$/A) and point-on-wave ($t_{\rm POW}$/ms into waveform). A number of features can be identified on these graphs. There is a "valley" of negative values (material loss) on the cathode 3-D plot at $t_{\rm POW} \sim 2$ ms across most $I_{\rm rms}$ values. Correspondingly, on the anode 3-D plot there is a "mountain range" of positive values (material gain) across most $I_{\rm rms}$ values. Also, the anode shows a large loss of material at $t_{\rm POW} \sim 5$ ms at high current values. A net zero mass loss can be estimated by extrapolating the 3-D plot Fig. 5(a) and the contour plot Fig. 5(c) of the cathode. Also, a net zero mass loss can be interpolated on the 3-D plot Fig. 5(b) and contour plot Fig. 5(d) of the anode across all current shown.

2) Ag/CdO Anode and Cathode at 0.1 ms^{-1} Opening Velocity: The mass change data, M_a, of Ag/CdO anodes and cathodes at 0.1 ms^{-1} opening velocity are shown in 3-D and contour plots in Fig. 6. The experimental data have been presented in a previous paper [20]. Similar features to the Ag/SnO_2 mass change data can be seen in this data. There is a "valley" of negative values (material loss) on the cathode 3-D plot at $t_{\rm POW} \sim 2$ ms across most $I_{\rm rms}$ values. Correspondingly, on the anode 3-D plot there is a "mountain range" of positive values (material gain) across mast $I_{\rm rms}$

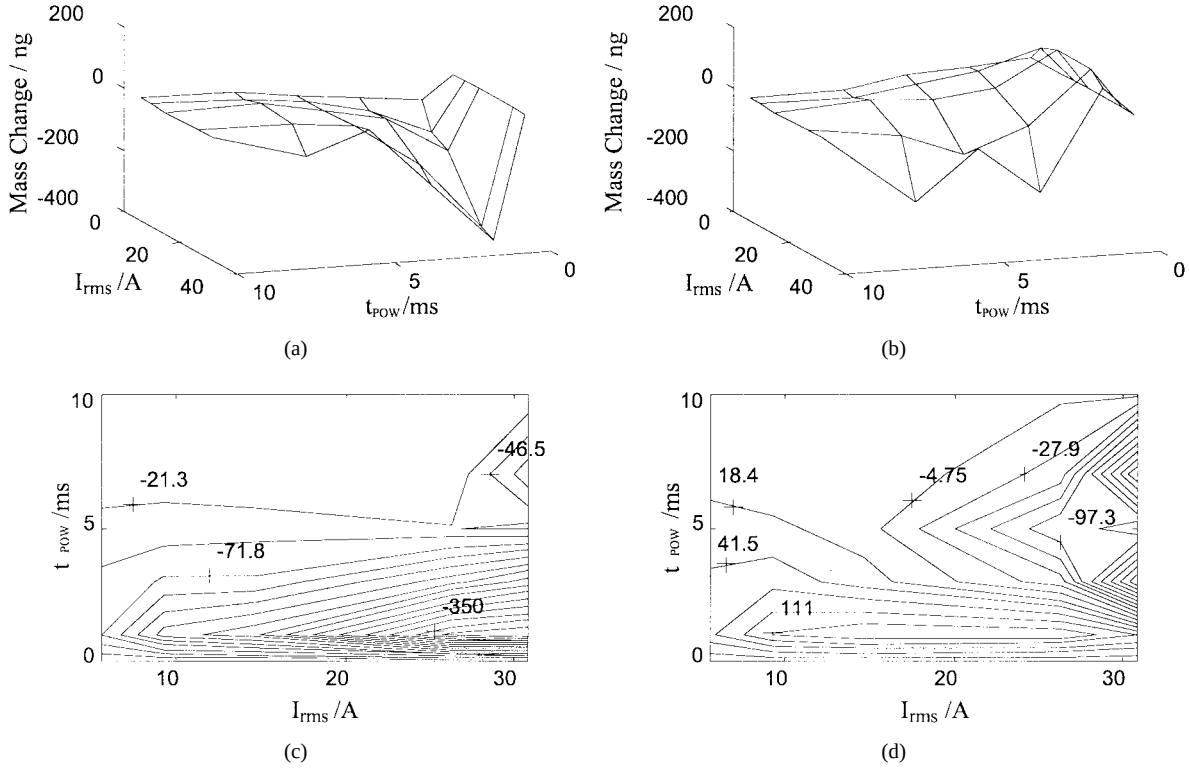

Fig. 5. Mass change (erosion) data for Ag/SnO_2 contacts.

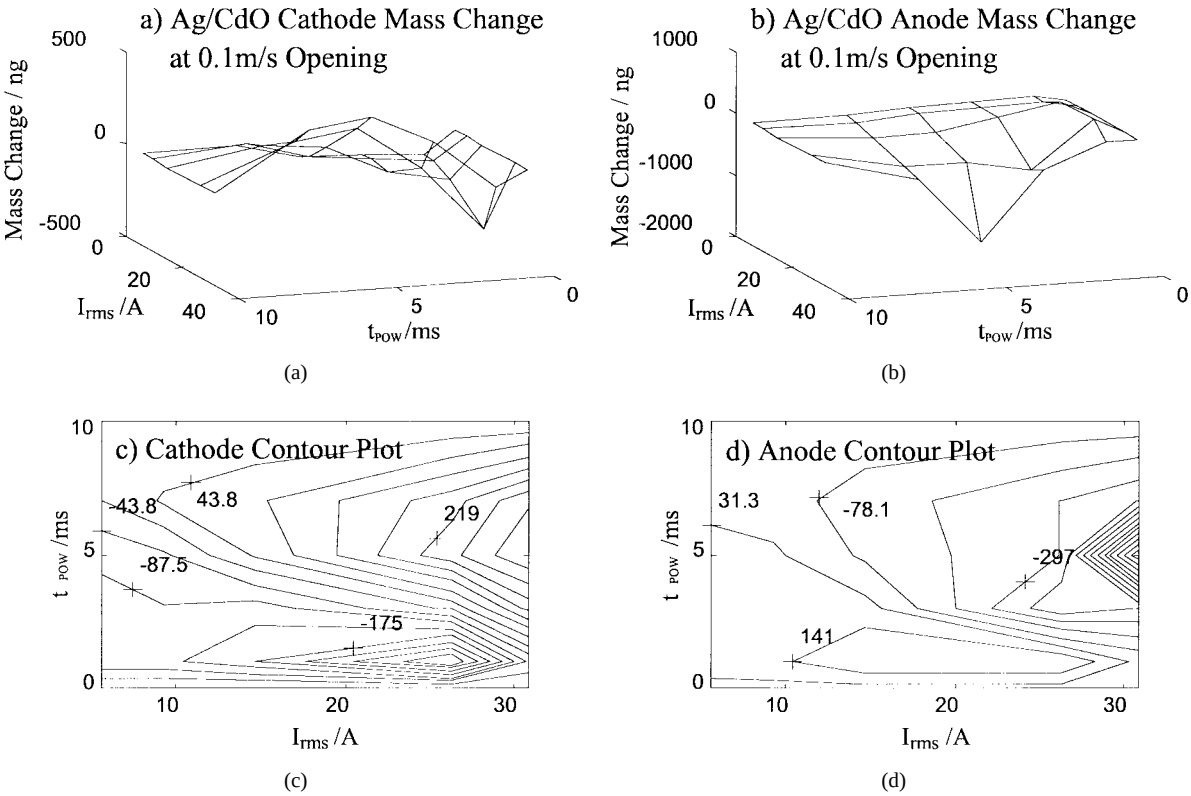

Fig. 6. Mass change (erosion) data for Ag/CdO contacts.

values. The anode shows a large loss of material at $t_{\mathrm{POW}} \sim 5$ ms at high current values which corresponds to a gain of material on the cathode at this point in the $I_{\mathrm{rms}}t_{\mathrm{POW}}$ plane. Areas of zero mass change can be interpolated on these plots. Comparing the mass change data of the anode and cathode shows an "imaging effect" in the mass change data on the $I_{\mathrm{rms}}t_{\mathrm{POW}}$ plane: a gain on one contact at particular I_{rms} and t_{POW} value produces a loss on the other, and visa versa.

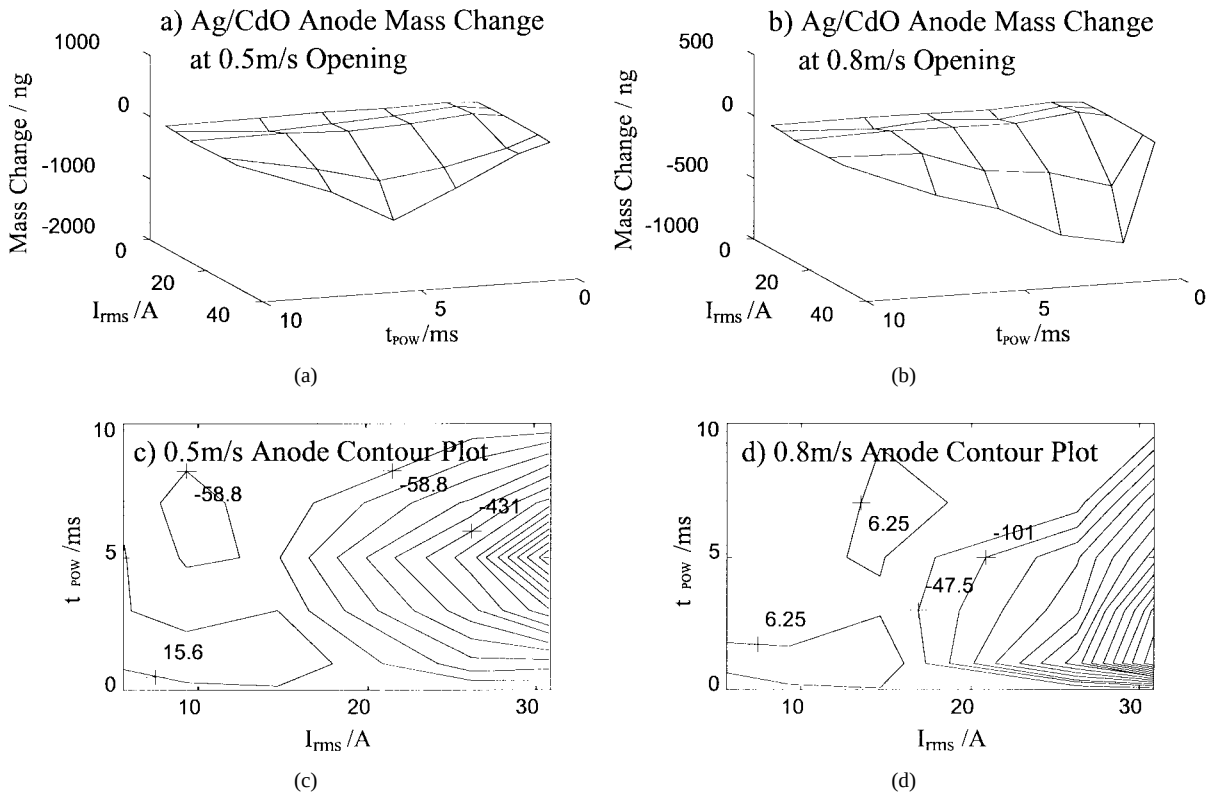

Fig. 7. Mass change (erosion) data for Ag/CdO anodes at different opening velocities.

Comparing the anode mass change data of Ag/SnO_2 [Fig. 5(b) and (d)] and Ag/CdO [Fig. 6(b) and (d)] samples shows similarities in the positions of mass loss and gain on the $I_{\rm rms}t_{\rm POW}$ plane.

3) Ag/CdO Anode Between 0.1–0.8 ms^{-1} Opening Velocity: The effect of opening velocity of the contact pair is also investigated using Ag/CdO rivets. Mass change data, M_a, is collected (holders were included in the mass measurement) for velocities of 0.1, 0.3, 0.5, 0.7, and 0.8 ms^{-1} and typical anode data is presented in Fig. 7.

By increasing the velocity from 0.1 to 0.8 ms^{-1} does not eliminate the "imaging effect" between the anode and cathode mass change profile (data not presented). A gain on one contact at particular $I_{\rm rms}$ and $t_{\rm POW}$ value produces a loss on the other, and visa versa.

Fig. 7 shows mass change data for anodes at 0.5 and 0.8 ms^{-1} opening velocities. By increasing the velocity causes the "mountain range" of material gain to move to lower current in the $I_{\rm rms}t_{\rm POW}$ plane. The magnitude of the material gain decreases with increasing velocity. The area of large loss moves to lower $t_{\rm POW}$ values with increasing velocity.

IV. The Zeta Characteristic, ζ

Figs. 8–10 are mass change schematics of the mass loss and deposition data presented in the previous section designed to show general features only and to draw attention to the significant features in the experimental data. These schematics are contour plots with the abscissa as current (rms), $I_{\rm rms}$/A, and the ordinate as point-on-wave, $t_{\rm POW}$/ms. The schematics show areas of mass loss and gain on the $I_{\rm rms}t_{\rm POW}$ plane indicated by the shaded discs. A bold line indicates the zeta characteristic, ζ, which is the arc duration resulting in net zero mass change. This has been extrapolated or interpolated from the experimental data. This arc duration is given on the second ordinate as $\zeta = \tau - t_{\rm POW}$ in the schematic. In positioning the ζ line on the schematic diagram, it is sketched to intercept the ordinate at $t_{\rm POW} < 10$ ms. This is because the metallic ion transfer mechanism first dominates the arc, even at low current, resulting in a finite amount of material being lost from the anode and deposited on the cathode.

Fig. 8 contains two mass change schematics corresponding to the anode and cathode Ag/SnO_2 mass change data (Fig. 5). The anode mass change schematic [Fig. 8(b)] contains a material loss "hole" and a material gain "mountain range" as shown. The ζ characteristic is shown giving required arc duration and $I_{\rm rms}$ for net zero mass loss. Net zero mass loss occurs when the effect of the metallic ion transfer mechanism and the gaseous ion transfer mechanism are in balance, equal, and opposite. To obtain a net zero mass change for a given current, a $t_{\rm POW}$ can be selected. The cathode mass change schematic [Fig. 8(a)] shows mainly material losses cathode ζ characteristic [Fig. 8(a)] has a different profile to the anode [Fig. 8(b)] and will be discussed later.

Fig. 9 contains two mass change schematics of Ag/CdO contacts (Fig. 6). The anode and cathode mass charge schematics can be seen to have similar features. There is material gain at low $t_{\rm POW}$ (beginning of the duty cycle) on the anode and losses on the cathode from low to high current values. There is a large loss at high current and $t_{\rm POW} \sim 5$ ms for the anode whereas there is gain for the cathode. A net zero

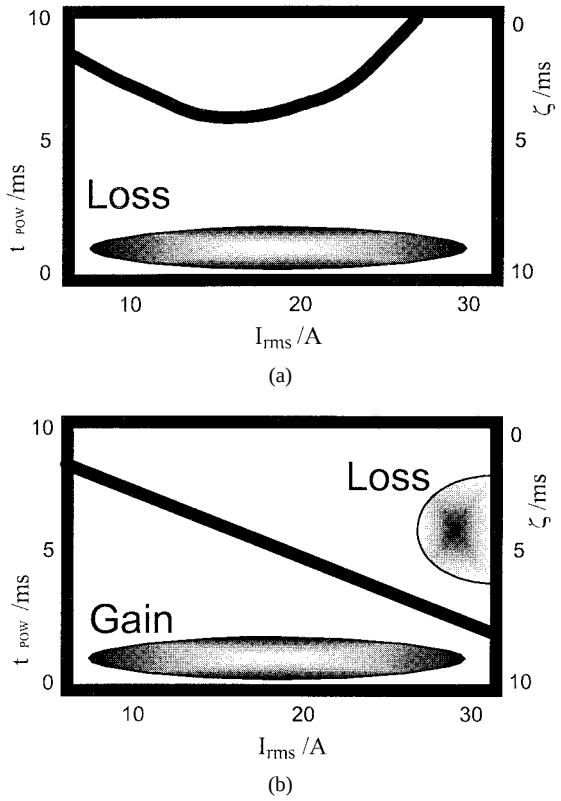

Fig. 8. Ag/SnO_2 mass change schematic.

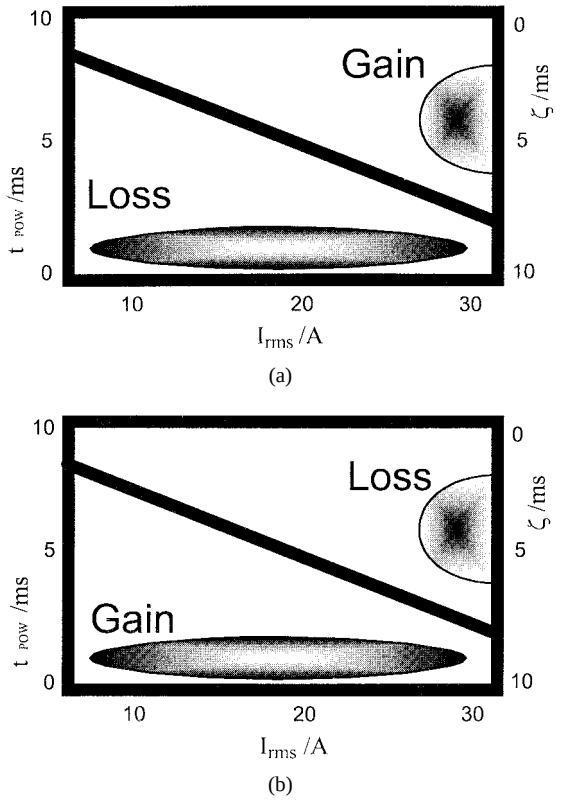

Fig. 9. Ag/CdO mass change schematic.

mass change characteristic is shown and is the same profile for both anode and cathode. The "imaging" effect can be seen between Fig. 9(a) and (b).

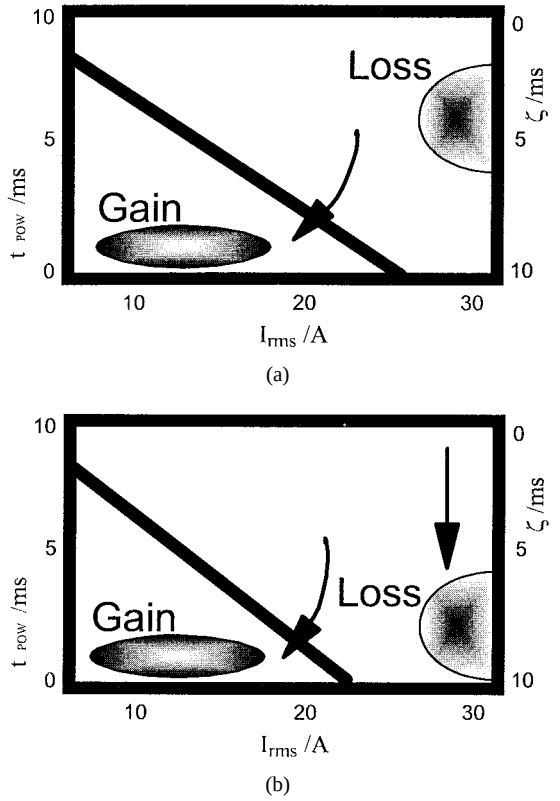

Fig. 10. Ag/CdO mass change schematic at different opening velocities.

Ag/SnO_2 and Ag/CdO anode schematics show the same general features. The ζ characteristic has a similar profile with high t_{POW} at low I_{rms} and low t_{POW} at high I_{rms}.

In the Ag/SnO_2 study only the contact rivets are weighed, whereas in the Ag/CdO study, contacts and holders are weighed so that deposits collected on the holder are included in the mass measurement. The effect of the different measuring techniques can be seen in comparing the cathodes in Figs. 8(a) and 9(a). In the Ag/CdO study which includes the holders, effectively all material is accounted for in this measurement. The material which is lost from the anode is deposited on the cathode contact or holder. In the Ag/SnO_2 study, only the contact was weighed, if any material is lost from the anode and collected on the cathode holder it would not be recorded in the data. This is seen on the Ag/SnO_2 cathode schematic Fig. 8(a), where a lot of material is lost at longer arcs and higher current.

Fig. 10 contains two schematic of anode mass change at 0.5 and 0.8 ms^{-1} (cf. Fig. 7) to illustrate the effect of opening velocity. Increasing the opening velocity from 0.1 to 0.8 ms^{-1} [cf. Fig. 5(b) and (d) and 7] causes the mass gain region on the schematic to be confined to lower current. The increase of velocity between 0.5 to 0.8 ms^{-1} (cf. Fig. 7) also causes the mass loss "hole" to move to a lower t_{POW} value. The position of the zeta characteristic on the $I_{\mathrm{rms}}t_{\mathrm{POW}}$ plane is also influenced by the opening velocity as shown. The experimental data [Fig. 7(b) and (d)] indicates that the zeta characteristic does not intercept the ordinate at $<$10 ms. However, the zeta characteristic has been sketched in Fig. 10(b) to intercept the ordinate at $<$ 10 ms for reasons given previously. This

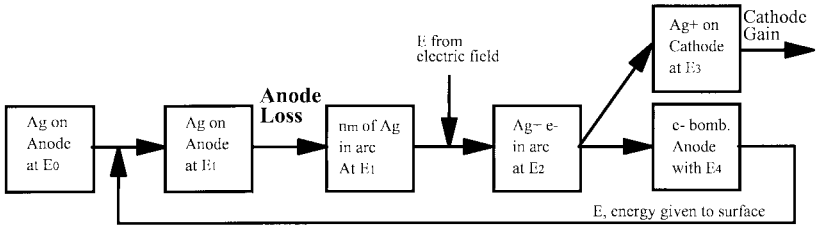

Fig. 11. Metallic ion transfer mechanism.

discrepancy is thought to be due to mass measurement errors. For zero mass loss at a given current (e.g., 20 A in Fig. 10), the arc duration (smaller t_{POW}) increases with velocity.

V. Discussion of the Zeta Condition

The aim of this discussion is to relate the zeta characteristic to experimental parameters. Three parameters are considered:

1) current;
2) arc duration;
3) contact opening velocity.

The discussion is focused on the anode but a similar analysis can be applied to the cathode.

As the arc discharge is drawn between opening contacts, it passes through two phases, the metallic phase at ignition and gaseous phase, before extinguishing. In the metallic phase the plasma is dominated by ionized metal vapor released from the contacts resulting in the metallic ion transfer mechanism dominating. In the gaseous phase the plasma is dominated by ionized gas from the environment resulting in the gaseous ion transfer mechanism dominating. It should be noted that each mechanism may partially take place outside the phase in which it dominates. As a consequence, from a mechanistic perspective, it is more useful to discuss the metallic and gaseous ion transfer mechanisms as opposed to metallic and gaseous phases. Each mechanism has its own distinctive mass removal rate and deposition rate at particular times, t. During the metallic phase the metallic ion transfer mechanism dominates so that the rate of mass removal at the anode, $(d\varepsilon_m(t))/dt$, is larger than the rate of anode mass deposition, $(dDg(t))/dt$. Opening the contact further, permits environmental gas to enter the arc affecting the $(dDg(t))/dt$ rate. The arc enters its gaseous phase when the gaseous ion transfer mechanism dominates so that the anode deposition rate becomes larger than the removal rate. The rate of mass change on the anode over the opening operation can be given by the expression in

$$\frac{dM_a(t)}{dt} = \frac{dD_g(t)}{dt} - \frac{d\varepsilon_m(t)}{dt}. \tag{1}$$

A. Anode Mass Removal Rate

The metallic ion transfer mechanism dominates at the beginning of the arc discharge but continues to occur throughout. A diagram of this mechanism is shown in Fig. 11 illustrating the path of silver particles from the anode into the arc discharge. Silver particles initially start in the anode material at room temperature (or at thermal energy E_0 in Fig. 11). Arc ignition and electron emission processes have been neglected for simplicity of this discussion. During an arc discharge the anode surface is heated by several mechanisms (electron bombardment being one) to a thermal energy E_1 as in Fig. 11. Consequently n_m number of silver particles (vapor) are released into the arc discharge. In the arc discharge the silver particles are ionized (e.g., by electron bombardment) and Ag ions and electrons are accelerated toward their respective electrodes. However, not all silver particles will ionize. The Saha equation can by used to determine the degree of ionization of the vapor. Energy for ionization and acceleration comes from the applied electric field and is indicated in Fig. 11. The electrons are accelerated toward the anode gaining energy (E_4 in Fig. 11) and bombard the anode delivering energy to the surface. This is illustrated in Fig. 11 by the feedback arrow with the label "E" indicating energy input to the surface. The ability for metal vapor to be released into the plasma increases the amount of subsequent ions and electrons for the metallic ion transfer mechanism.

Equation (2) relates the anode mass removal rate caused by the metallic ion transfer mechanism to power by the metallic transfer function, $R_m(I_{\mathrm{rms}})$

$$\frac{d\varepsilon_m(t)}{dt} = R_m(I_{\mathrm{rms}})P(I_{\mathrm{rms}}, t). \tag{2}$$

The metallic transfer function represents the mass removal efficiency of a single incident particle (an electron), k_{eff}, from the anode surface by bombardment and the number density of incident particles precursors, n_m as indicated in Fig. 11 (the number density of metallic atoms which result in metallic ions and electrons). Increasing the power of the system increases the degree of ionization of the vapor (the number density of ions and electrons) and the energy the electron can deliver to the surface in a given time period. More material is released into the gap when more energy is given to the surface. The influence of the three parameters under consideration on the density of metal vapor, n_m, is given below:

1) Current: Increasing the current increases the number of electrons and electron density assuming the arc cross-sectional area remains constant. Increasing the density of electrons increases the probability of bombardment of the anode surface and thus increases the amount of material (silver) evaporation. Therefore, R_m is assumed to be a function of I_{rms}.

2) Arc Duration: The number density of silver particles released from the surface in a particular time is thought not to be influenced by the duration of energy input into that surface (assuming thermal equilibrium of the surface).

3) Opening Velocity: Opening velocity is assumed not to have a significant effect on the number of silver particles released from the surface.

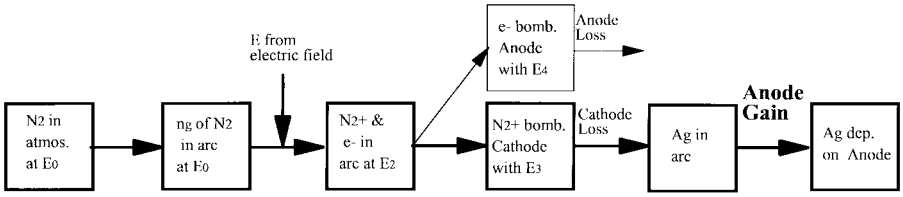

Fig. 12. Gaseous ion transfer mechanism.

B. Anode Mass Gain Rate

The gaseous ion transfer mechanism occurs once gaseous ions diffuse into the arc but may not dominate the arc behavior. Once atmospheric gaseous have diffused into the arc discharge in large numbers and have a greater influence over the arc than silver vapor, the gaseous ion transfer mechanism dominates the arc behavior. A diagram of the mechanism is given in Fig. 12 where the path of a gaseous species (nitrogen) is followed. The nitrogen molecules originate in the environment at room temperature (signified by thermal energy E_0 in Fig. 12) surrounding the arc. They diffuse into the arc at a rate given by a diffusion constant so that at a given time n_g number of nitrogen molecules will be found in the discharge (as indicated in Fig. 12). The diatomic nitrogen gas can undergo disassociation and several levels of ionization once in the discharge. In Fig. 12 only primary ionization of the molecule is considered for simplicity giving N_2^+ and an electron. A typical arc (containing molecular nitrogen) at 1 atmosphere pressure and 13 000K would be 10% ionized [22]. These ions and electrons are accelerated to their respective electrode. The energy for ionization and acceleration comes from the applied electric field and is indicated in Fig. 12. The electrons from nitrogen ionization supplement the electrons from the dwindling supply of silver metal (due to contact opening) and bombard the anode. The N_2^+ species bombard the cathode releasing new silver atoms to the discharge which can deposit on the anode, transferring material from the cathode to the anode. It should be noted that any silver atoms in the arc discharge can either:

1) be lost to the environment;
2) redeposit back onto the originating cathode by condensation;
3) deposit onto the anode by condensation.

Equation (3) relates the anode mass gain rate caused by the gaseous ion transfer mechanism to power by the gaseous transfer function, $R_g(t, v^{-1})$

$$\frac{dD_g(t)}{dt} = R_g(t, v^{-1})P(I_{\rm rms}, t). \tag{3}$$

The gaseous transfer function represents the mass removal efficiency of a single incident particle (N_2^+), $k_{\rm eff}$, from the cathode surface by bombardment and the number density of incident particles precursors, n_g as indicated in Fig. 12 (the number density of gaseous molecules resulting, e.g., in N_2^+ species). Increasing the power of the system increases ionization and the number density of ions, and the energy the ions can deliver to the surface in a given time period. The influence of the three parameters under consideration on the gaseous density in the arc, n_g, is given below:

1) Current: The current is assumed not to have an influence the amount of atmospheric gas which can diffuse into the arc discharge. Other factors such as increasing atmospheric pressure may influence the amount of gas which can diffuse into the discharge.

2) Arc Duration: The arc duration is assumed to have an influence on the gaseous ion density. The longer the arc is exposed to an atmosphere the larger the amount of gas that can diffuse into the arc, depending upon the diffusion constant and saturation limit.

3) Opening Velocity: The opening velocity is assumed to have an influence on the amount of gas that can diffuse into the arc. The diffusion constant governs that rate at which gases can diffuse into the arc and by increasing the rate of contact opening gives less time for the gas to enter the arc for a given gap and arc volume. Thus lowering the number density of gaseous particle which diffuse into the arc.

C. At the Zeta Condition

When the amount of mass loss on the anode is equal to the amount of deposition, net zero mass loss, this is considered to be the zeta condition. This can be represented as in (4), setting the mass change to zero and integrating between $t_{\rm POW}$ and the end of the waveform τ, where arc duration $\zeta = \tau - t_{\rm POW}$. Both R_g and R_m coefficients are integrated across the whole arc duration as both the metallic and gaseous ion transfer mechanisms occur throughout the arc duration

$$M_a = 0 = \int_{t=\tau-\zeta}^{\tau} (R_g(t, v^{-1}) - R_m(I_{\rm rms}))P(I_{\rm rms}, t)\,dt. \tag{4}$$

As a first approximation, the metallic transfer function is assumed to have a linear relationship to current, and the gaseous transfer function is assumed to have a linear relationship to arc duration and an inverse relationship to opening velocity. Equation (4) is rearranged and integrated, as in the Appendix, to give (5)

$$\zeta = 2KvI_{\rm rms} \tag{5}$$

where the K is a constant of proportionality.

This equation shows that the arc duration required to produce a net zero mass loss is directly proportional to opening velocity and current. A closer look at the metallic and gaseous ion transfer mechanisms, assuming (2) and (3) apply, confirms this. Fig. 13(a) contains plots of (2) and (3) of anode mass removal rate and anode mass gain rate, respectively, and the sum of these know as the mass change rate, for opening velocity of 0.1 ms^{-1}. Fig. 13(b) contains the loss, gain and the sum of these two know as the mass change for this velocity.

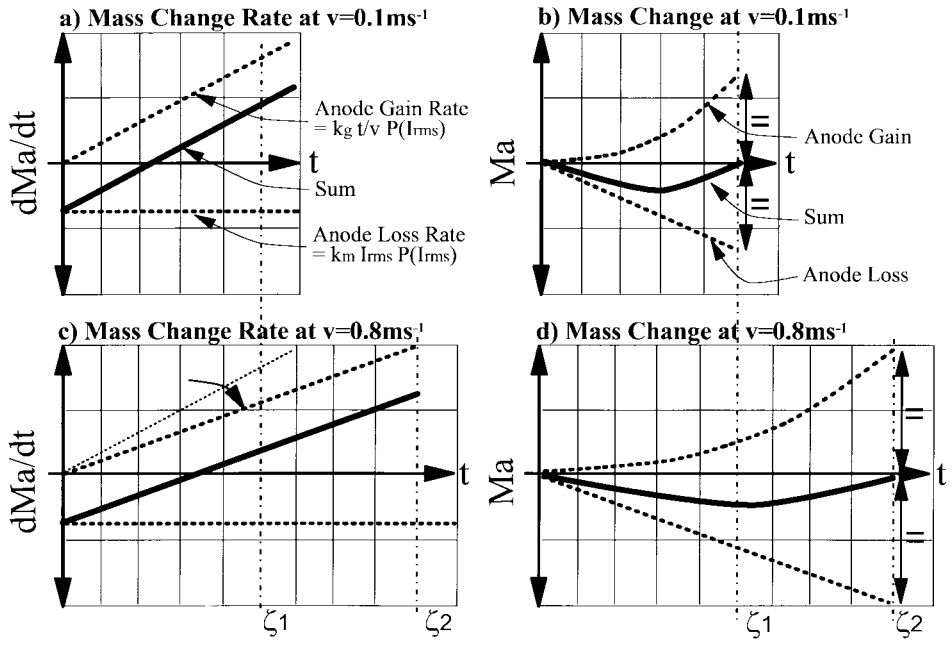

Fig. 13. Mass change rate and mass change at two velocities.

Fig. 13(c) and (d) corresponds to a velocity of 0.8 ms^{-1}. The mass change rate on the anode is the sum of the removal rate due to the metallic ion transfer mechanism and the gain rate due to the gaseous ion transfer mechanism. The anode loss rate is constant as a constant current is assumed for a first approximation (see the Appendix). The anode gain rate increase with time as gaseous ions diffuse into the arc. The total amount of mass change on the anode [Fig. 13(b)] is the sum of the total amount of material removed and the total amount of material deposited. These terms come from integrating the rate terms used in Fig. 13(a). Fig. 13(b) shows the zeta condition, ζ_1, when the total amount of material deposited is equal to the total amount of materials lost at an opening velocity of 0.1 ms^{-1}. Fig. 13(d) shows the zeta condition, ζ_2, when the total amount of material deposited is equal to the total amount of materials lost at an opening velocity of 0.8 ms^{-1}. It can be seen that increasing the velocity decreases the rate of deposition [Fig. 13(c)] and thus the zeta condition $\zeta_2 > \zeta_1$.

The general behavior of (5) can be verified by comparing this equation to the experimental data for different current and velocity. K was found from the experimental study by taking an approximate gradient of the ζ characteristic with current for 0.1 ms^{-1} opening velocity ($\sim 1.3 \times 10^{-4}$ sA^{-1}). This was found to be $\sim 1.3 \times 10^{-3}$ $\text{s}^2\text{m}^{-1}\text{A}^{-1}$. Fig. 14 is a plot of (5), ζ against v and I_{rms}, using this value of K. The bold line shown on the plot at $v = 0.1$ ms^{-1} in Fig. 14 indicates the net zero mass loss at an opening velocity of 0.1 ms^{-1}. It can be seen in Fig. 14 that for velocities above 0.1 ms^{-1}, the zeta characteristic follows a similar behavior to the observed data. At higher velocity, the zeta characteristic gradient increases so that net zero mass loss can only be achieved at low current. Fig. 14 also predicts what might be expected for the arc duration for net zero mass loss at lower opening velocities 0.03 ms^{-1}.

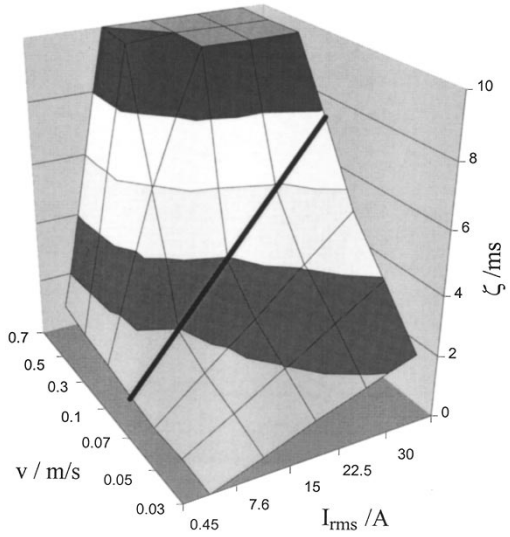

Fig. 14. Model of the zeta characteristic at different current and opening velocities.

VI. Conclusion

Studies are conducted on silver metal oxide contacts on a purposed built apparatus to investigate the extent of contact erosion under opening (break) operations. Ag/SnO_2 and Ag/CdO contact rivets are studied with alternating current up to 30 A rms, contacts opened at particular point-on-wave, and at different opening velocities between 0.1–0.8 ms^{-1}.

On opening the contacts, the arc discharge forms between the contact rivets and remains on the contacts until extinguished—there is no evidence that the arc formed on the holders. The contacts show extensive erosion depending upon current and arc duration. Any one particular contact not only undergo mass loss during a discharge but also mass gain. In addition, material deposition is clearly seen on the contact

holders indicating that some contact material radially expands from the arc discharge.

At opening velocity of 0.1 ms^{-1}, cathodes of both Ag/CdO and Ag/SnO_2 lose material at low t_{POW} with I_{rms} between 1–30 A. However, anodes gained material over this section on the $I_{\mathrm{rms}}t_{\mathrm{POW}}$ plane. A similar feature is seen at high I_{rms} and $t_{\mathrm{POW}} \sim 5$ ms, where material is gained on the cathode and lost on the anode. The zeta characteristic of net zero mass loss against the $I_{\mathrm{rms}}t_{\mathrm{POW}}$ plane is the same for both anode and cathode, and Ag/SnO_2 and Ag/CdO as long as the contact holders are included in the mass measurement.

The opening velocity has an influence on the zeta characteristic. Increasing the velocity results in the requirement for longer arc duration (smaller t_{POW}) at same current for net zero mass loss.

APPENDIX

Power is the product of the voltage drop across the arc and the supply current, which is a function of time for ac as in

$$P(I_{\mathrm{rms}}, t) = V\sqrt{2}I_{\mathrm{rms}} \sin(wt). \tag{A1}$$

Equation (4) is rearranged to give (A2). However, for a first approximation and to simplify the expressions, power is consider to be the function of I_{rms} only and the limits have been modified so that t_{POW} is set to $t = 0$, integrating through to $t = \zeta$, as shown

$$\int_{t=0}^{\zeta} R_g(t, v^{-1})P(I_{\mathrm{rms}})\,dt = \int_{t=0}^{\zeta} R_m(I_{\mathrm{rms}})P(I_{\mathrm{rms}})\,dt. \tag{A2}$$

The metallic ion mechanism rate function is assumed to have a linear relationship to current and is related by a constant k_m. The gaseous ion mechanism rate function is assumed to have a linear relationship to arc duration and an inverse relationship to the constant k_g. These are substituted into (A2) to give

$$\int_{t=0}^{\zeta} k_g \frac{t}{v} P(I_{\mathrm{rms}})\,dt = \int_{t=0}^{\zeta} k_m I_{\mathrm{rms}} P(I_{\mathrm{rms}})\,dt. \tag{A3}$$

This is integrated to give

$$\frac{k_g P(I_{\mathrm{rms}})}{v} \frac{1}{2} (\zeta^2 - (0)^2) = k_m I_{\mathrm{rms}} P(I_{\mathrm{rms}})(\zeta - 0). \tag{A4}$$

Dividing both sides by $P(I_{\mathrm{rms}})$ and rearranging gives

$$\zeta = 2\frac{k_m}{k_g} v I_{\mathrm{rms}}. \tag{A5}$$

This equation is simplified and presented in (5).

REFERENCES

[1] R. Holm, *Electric Contacts*, 4th ed. New York: Springer-Verlag, 1967.

[2] H. N. Wager, "Performance principles of switching contacts," in *Physical Design of Electronic Systems: Integrated Devices and Connection Technology*, D. Baker, Ed. Englewood Cliffs, NJ: Prentice-Hall, 1971, pp. 500–594.

[3] Z.-K. Chen, H. Mizukoshi, and K. Sawa, "Contact resistance characteristics of Ag material in breaking low-load DC arcs," *IEEE Trans. Comp., Packag., Manufact. Technol. A*, vol. 17, pp. 113–129, Mar. 1994.

[4] ———, "Contact erosion patterns of Pd materials in DC breaking arcs," *IEEE Trans. Comp., Packag., Manufact. Technol. A*, vol. 17, pp. 61–67, Mar. 1994.

[5] Z.-K. Chen and K. Sawa, "Effect of arc behavior on material transfer: A review," *IEEE Trans. Comp., Packag., Manufact. Technol. A*, vol. 21, pp. 310–322, June 1998.

[6] J. Swingler and J. W. McBride, "The erosion and arc characteristics of Ag/CdO and Ag/SnO_2 contact materials under DC break condition," *IEEE Trans. Comp., Packag., Manufact. Technol. A*, vol. 19, pp. 404–415, Sept. 1996.

[7] N. B. Jemaa, J. L. Queffelec, and D. Travers, "Theoretical multisite operating arc model applied to statistical arc duration measurement on break at low electrical level," in *Proc. IEEE Holm Conf. Elect. Contacts*, 1984, pp. 573–579.

[8] N. B. Jemaa, L. Nedelec, and S. Benhenda, "Anodic and cathodic erosion of Ag, Ag alloys and Ag–MeO contacts materials in energy range below 10 joules," in *Proc. IEEE Holm Conf. Elect. Contacts*, 1996, pp. 70–73.

[9] P. J. Boddy and T. Utsumi, "Fluctuations of arc potential caused by metal-vapor diffusion in arcs in air," *J. Appl. Phys.*, vol. 42, no. 9, pp. 3369–3373, 1971.

[10] H. Hoft, "Contribution to the calculation of arc breakdown voltage," in *Proc. Int. Conf. Elect. Contacts*, 1982, pp. 383–386.

[11] N. Ben Jemaa, "Contributions a l'etude des arcs electriques d'ouverure de circuits basse tension et au viosinage du zero de courant dans contacts electriques seperables," Ph.D. dissertation, Rennes Univ., France, 1985.

[12] N. Ben Jemaa, J. L. Queffelec, and D. Travers, "Some investigations on slow and fast arc voltage fluctuations for contact materials proceeding in various gases and direct current," in *Proc. IEEE Holm Conf. Elect. Contacts*, 1990, pp. 18–24.

[13] J. W. McBride and S. M. Sharkh, "Arc voltage fluctuations at low current," in *Proc. Int. Symp. Electrical Contacts Theory and Appl., ISECTA'93*, Alma-Alta, Kazakhstan, June 1993, pp. 53–59.

[14] M. R. Hopkins and R. H. Jones, "Transients, bridges, micro-arcs and metal transfer in low voltage electrical contacts," in *Proc. IEEE Holm Conf. Elect. Contact Phenom.*, 1972, pp. 401–406.

[15] Z. K. Chen, "Material transfer and contact resistance deterioration in light duty electrical contacts," Ph.D. thesis, Keio Univ., Yokoha, Japan, 1995.

[16] Z. K. Chen and K. Sawa, "Particle sputtering and depositing mechanism for material transfer in breaking arcs," *J. Appl. Phys.*, vol. 76, pp. 3326–3331, 1994.

[17] N. Ben Jemaa, L. Morin, S. Benhenda, and L. Hedelec, "Anodic to cathodic arc transition according to break arc lengthening," *IEEE Trans. Comp., Packag., Manufact. Technol.*, to be published.

[18] J. W. McBride, K. J. Cross, and S. M. Sharkh, "The evaluation of arc erosion on electrical contacts using three-dimensional surface profiles," *IEEE Trans. Comp., Packag., Manufact. Technol. A*, vol. 19, pp. 87–97, Mar. 1996.

[19] J. W. McBride and S. M. Sharkh, "The influence of contact opening velocity on arc characteristics," in *Proc. 16th Int. Conf. Elect. Contacts*, 1992, pp. 395–400.

[20] S. M. Sharkh and J. W. McBride, "A comparison between AC and DC erosion of Ag/CdO contacts," in *Proc. 17th Int. Conf. Elect. Contacts*, 1994.

[21] S. M. AbuSharkh, "Influence of contact dynamics and point-on-wave switching on arc and contact phenomena in medium duty switches," Ph.D. thesis, Univ. of Southampton, U.K., 1994.

[22] S. C. Brown, *Introduction To Electrical Discharge in Gases.* New York: Wiley, 1966.

Jonathan Swingler received the joint honors degree in physics and chemistry from the University of Keele, U.K., in 1990 and the Ph.D. degree in electrical contact science and technology from Loughborough University, U.K., in 1994.

His Ph.D. research was primarily concerned with degradation processes at connector contact surfaces and the influence of lubricants in improving contact performance. After this, he moved to Southampton to investigate contact materials for medium duty switching, arc modeling, hybrid switching, constriction resistance measurement, and connector reliability. He is a Senior Research Fellow at the University of Southampton.

Dr. Swingler is a Chartered Physicist, a Member of the Institute of Physics, and an Associate Member of the Institute of Electrical Engineers.

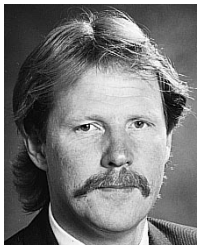

John W. McBride received the degree in aeronautical engineering from the University of Southampton, U.K., in 1978 and the Ph.D. degree in electrical contact phenomena from Plymouth University, U.K., in 1986.

From 1985 to 1987, he lectured in the Mechanical Engineering Department, Plymouth University, and since 1987, he has been a Lecturer and Senior Lecturer since 1995 in Instrumentation and Electro-Mechanical Design in the Departments of Mechanical and Electrical Engineering, University of Southampton. His main research interests include electrical contacts, metrology, and instrumentation.

Dr. McBride is a member of the IEE, a Chartered Engineer, Head of Research in Mechanical Engineering, and Chair of the Electro-Mechanical Research Group.